

The mean surface circulation of the North Atlantic subpolar gyre: A comparison of estimates derived from new gravity and oceanographic measurements

S. Higginson,¹ K. R. Thompson,¹ J. Huang,² M. Véronneau,² and D. G. Wright³

Received 13 December 2010; revised 13 April 2011; accepted 23 May 2011; published 20 August 2011.

[1] A new mean sea surface topography (MSST) is used to estimate the surface circulation of the subpolar gyre of the northwest Atlantic. The MSST is produced using a new geoid model derived from a blend of gravity data from the Gravity Recovery and Climate Experiment (GRACE) satellite mission, satellite altimeters, and terrestrial measurements. The MSST is compared with a topography produced by an ocean model which is spectrally nudged to a new Argo period temperature and salinity climatology. The mean surface circulation associated with the geodetic MSST is compared with estimates of the circulation from surface drifters, moorings, and other in situ measurements. The geodetic MSST and circulation estimate are found to be in good agreement with the other estimates, both qualitatively and quantitatively. The topography is found to be an improvement over an earlier geodetic estimate with better resolution of the coastal currents. Deficiencies are identified in the ocean model's estimate of flow over shelf regions.

Citation: Higginson, S., K. R. Thompson, J. Huang, M. Véronneau, and D. G. Wright (2011), The mean surface circulation of the North Atlantic subpolar gyre: A comparison of estimates derived from new gravity and oceanographic measurements, *J. Geophys. Res.*, 116, C08016, doi:10.1029/2010JC006877.

1. Introduction

[2] The dominant large-scale feature of the surface circulation of the northwest Atlantic is the subpolar gyre. This cyclonic circulation comprises a warm, salty poleward flow (an extension of the Gulf Stream) and a return fresh, cold flow along the shelf at the western edge of the basin [e.g., *Lazier and Wright*, 1993; *Heywood et al.*, 1994]. The warm northward flowing currents are the North Atlantic Current and the Irminger Current, and the colder return currents are the East Greenland Current, the West Greenland Current, and the Labrador Current. A simplified representation of the circulation is shown in Figure 1.

[3] The equatorward flowing currents of the subpolar gyre provide a pathway for the export of fresh water from high latitudes. Climate change may alter this freshwater flux, for example, changing sea ice cover, river discharge, Greenland melting, and the Arctic throughflow [*Dickson et al.*, 2007]. Modeling studies indicate that an increase in the freshwater flux can increase stratification of the interior of the subpolar gyre, including the Labrador Sea. This may reduce deep water formation and hence the strength of the meridional overturning circulation [*Gerdas et al.*, 2006; *Stouffer et al.*,

2006; *Smith and Gregory*, 2009]. *Smith and Gregory* [2009] show that the effect is sensitive to the region of freshwater forcing, and *Schmidt and Send* [2007] construct freshwater budgets that show that the West Greenland Current is likely the dominant source of summer fresh water to the surface layer of the interior Labrador Sea. Monitoring the impact of climate change requires that we have an understanding of the circulation.

[4] Although some southern parts of the gyre are well sampled, oceanographic observations of much of the gyre have been infrequent and biased toward the summer months because of geographic isolation and winter ice cover [*Bacon et al.*, 2008]. Several sections are regularly sampled, for example, the World Ocean Circulation Experiment (WOCE) AR7W line between the coasts of Labrador and Greenland, which is occupied annually by the Bedford Institute of Oceanography [*Yashayaev*, 2007]. Float deployments have been used to map the circulation and water properties, for example, the subsurface floats of the Labrador Sea Deep Convection Experiment [*Lavender et al.*, 2000]. Other sampling is sporadic and sparse; for example, *Fratantoni and Pickart* [2007] note only a handful of observations in the northern Labrador Sea between 1990 and 2001. Estimates of the mean circulation based on such sampling may be seasonally biased, and there may be significant aliasing of low-frequency variability.

[5] This study considers two techniques for estimating the mean surface circulation of this region, potentially reducing the uncertainties associated with sparse in situ measurements. First, the mean sea surface topography (MSST), also known as mean dynamic topography and dynamic ocean topography, can be determined geodetically. The geoid is a level of

¹Department of Oceanography, Dalhousie University, Halifax, Nova Scotia, Canada.

²Geodetic Survey Division, CCRS, Natural Resources Canada, Ottawa, Ontario, Canada.

³Fisheries and Oceans Canada, Bedford Institute of Oceanography, Dartmouth, Nova Scotia, Canada.

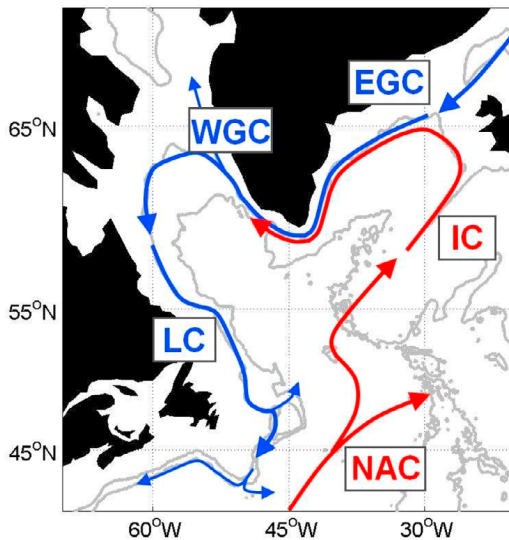


Figure 1. The major surface currents of the northwest Atlantic [after Lazier and Wright, 1993]. The labeled currents are the North Atlantic Current (NAC), the Irminger Current (IC), the East Greenland Current (EGC), the West Greenland Current (WGC), and the Labrador Current (LC). The grey lines are the 1000 and 3000 m isobaths.

equal gravitational potential which can be loosely defined as the mean sea level of the ocean at rest. In this study the geoid is modeled using a combination of measurements from the Gravity Recovery and Climate Experiment (GRACE) satellite mission, altimeters, and terrestrial gravity measurements. Subtracting the geoid from the mean sea surface height measured by satellite altimeters gives the MSST. The mean surface circulation is calculated from the gradients of the MSST, with no need for an assumed level of no motion. This approach was adopted by Rio and Hernandez [2004], Bingham et al. [2008], Thompson et al. [2009], and others. Thompson et al. [2009] produced an estimate of the mean circulation in the northwest Atlantic which compared favorably with independent observations along the coast of Labrador, but there were significant differences in the area around Greenland. Our study uses additional gravity data from the coastal ocean off Greenland, together with improved quality control of the gravity data, to overcome the shortcomings of this earlier study.

[6] The second technique considered is to derive the mean surface circulation from temperature and salinity (TS) profiles measured by the Argo program of subsurface floats. Argo floats are drifting profilers which measure temperature and salinity to a depth of approximately 2000 m every 10 days. We reduce the effect of mesoscale variability in the Argo measurements using the method of Higginson et al. [2009]. The adjusted Argo TS data are used to produce a climatology. Unlike existing TS climatologies, this new climatology relates to the relatively short period from 2000 to 2009. In this sense the climatology is more correctly described as a decadal mean. Dynamic height and the surface circulation can be calculated from a TS climatology, but this requires either a known reference velocity or the unrealistic assumption of a level of no motion in the deep ocean. Instead,

we spectrally nudge [Thompson et al., 2006] an ocean circulation model to the new climatology, thereby giving an oceanographic estimate of MSST and the surface circulation.

[7] The new estimates of MSST and their associated mean surface circulations are next compared and evaluated against independent sets of oceanographic observations. The most comprehensive set of observations is velocity measurements from the satellite-tracked surface-drifting buoys of the Global Drifter Program [Lumpkin and Pazos, 2007]. Additional direct velocity measurements are available from occasional oceanographic surveys, the regularly occupied sections such as AR7W, and moored buoys.

[8] This study has two key components that extend our understanding. First, the geodetically determined MSST incorporates additional gravity measurements to the data set used by Thompson et al. [2009], predominantly around Greenland. This should give better resolution of the relatively narrow East and West Greenland currents. Second, the oceanographic MSST is estimated using a new TS climatology based on data specific to the period 2000–2009. Previous climatologies are based on multidecadal observations, but the TS structure of the Labrador Sea has been observed to vary on decadal time scales [Yashayaev, 2007], so it is more appropriate to define the climatology for a shorter time period.

[9] The structure of the paper is as follows. The data and methods used for the geodetic estimate of MSST are described in section 2. The construction of the oceanographic estimate of MSST is discussed in section 3, together with a description of other oceanographic validation data. The comparison and evaluation of the two new estimates is described in section 4, and the new contributions from this study are discussed in section 5.

2. MSST From Altimeter and Gravity Observations

[10] In this section we describe the calculation of a geodetically determined MSST for the northwest Atlantic using a new geoid model and an altimeter-derived mean sea surface height. The mean sea surface (MSS) is described first, followed by the geoid model and then the resulting MSST.

2.1. Mean Sea Surface Height

[11] Satellite altimeters have been in orbit since the 1980s measuring the sea surface height relative to a reference ellipsoid. A continuous record exists since 1992 based on a number of missions, including the TOPEX/POSEIDON, ERS-1, ERS-2, and Jason 1 satellites. For this study we use the MSS_CNES_CLS10 mean sea surface product distributed by Archiving, Validation and Interpretation of Satellite Oceanographic data (Aviso). This MSS combines 16 years of altimeter data referenced to the 1993–1999 period and represents the geoid plus the MSST for this period. It is computed on a $\frac{1}{10}^\circ$ grid using altimeter data within a 200 km radius of each grid point. The resulting MSS, and an estimate of its error, are interpolated onto a nominal $\frac{1}{30}^\circ$ grid by Aviso. MSS values range from approximately -45 to $+70$ m in the region of this study, and the error estimate is typically less than 5 cm. Aviso relaxed the MSS toward an estimate of the geoid in the coastal zone (approximately 50 km from shore) because of the errors associated with satellite altimeter mea-

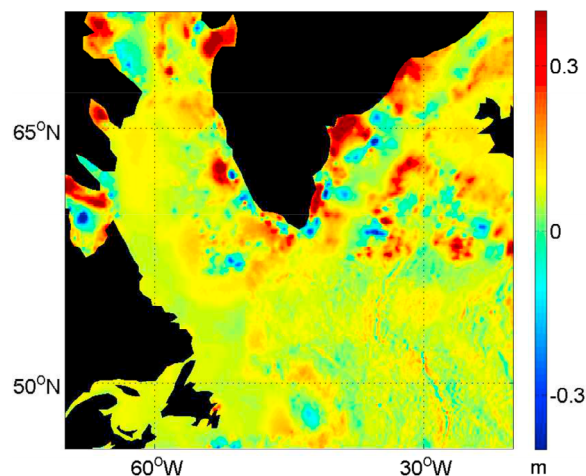


Figure 2. Difference in height between the PCG08I geoid model used in this study and the geoid model used by *Thompson et al.* [2009].

measurements near coastlines. We adjust the altimeter measurements so that the MSS represents the geoid plus the MSST for the period 2000–2009, corresponding with the reference period of the oceanographic estimate of MSST described in section 3.

2.2. Geoid Model

[12] We use the Preliminary Canadian Geoid Model 2008, version I (PCG08I), one of a series of experimental geoid models developed at Natural Resources Canada. This model covers all of North America (10°N–90°N, 170°W–10°W), but the focus of its development has been on Canadian territory and the neighboring oceans. For the rest of the study region Natural Resources Canada relies on data provided by external international agencies (e.g., U.S. National Geodetic Survey, U.S. National Geospatial-Intelligence Agency, and Danish Space Center), although additional validation procedures are applied.

[13] The geoid model is determined from a gravity field that is a composite of satellite gravity data, gravity derived from satellite altimetry, and terrestrial gravity data. The realization of the marine gravity grid for PCG08I follows the multistep approach described in Appendix A. The gridded gravity field represents an updated version of the grid published by *Thompson et al.* [2009]. The difference between the two grids exceeds 10 mGal in some areas around Greenland but is generally much less in other areas.

[14] The geoid model is computed from the gravity grid using the same methodology as described by *Thompson et al.* [2009]. The difference between the new model and the one used in their study exceeds 20 cm around the coast of Greenland (Figure 2) largely because of the use of newer Arctic Gravity Project (ArcGP) and altimeter-derived gravity grids. However, the difference is only a few centimeters along the Canadian east coast where basically the same gravity data set is used. The geoid errors range from a few centimeters to decimeters, but the total geoid error is mostly between 1 and 5 cm for the study area. A fuller description of the data sources, methods, and error estimation is included in Appendix A.

2.3. Mean Sea Surface Topography

[15] The mean sea surface topography is calculated by a pointwise subtraction of the new geoid model from the MSS_CNES_CLS10 mean sea surface adjusted to the 2000–2009 reference period. The MSST is mapped onto a $\frac{1}{4}^\circ$ grid by taking the mean of all values within $\pm\frac{1}{4}^\circ$ of each grid point. The MSS is relaxed toward a geoid model in the coastal zone (50 km or approximately $\frac{1}{2}^\circ$ from shore; see section 2.1), so we have chosen to exclude the MSST within $\frac{1}{4}^\circ$ of the coastline, where the geoid model dominates. The resulting topography (MSST_G) is shown in Figure 3. The appearance of the topography is largely as expected. The low of the cyclonic subpolar gyre is clearly visible to the south of Greenland, and the high associated with subtropical waters south of the Gulf Stream is just visible at the southern edge of the domain. It is encouraging that the new MSST is smoother than the topography produced by *Thompson et al.* [2009], which contained a number of spurious features near Greenland.

[16] The mean surface geostrophic speed is calculated from the gradients of MSST_G (Figure 4, top right). This shows the shelf break current along the coasts of Greenland and Labrador with the Gulf Stream extension just visible around 45°W. The corresponding speed calculated from the gradients of the topography discussed by *Thompson et al.* [2009], MSST_{GO}, is shown in Figure 4 (top left). A number of unexpected circulation features appear north of 55°N which do not appear in the speed plot derived from MSST_G.

3. Oceanographic Validation Data

[17] An ocean model and oceanographic observations are now used to estimate the MSST and the mean surface circulation.

3.1. Ocean Model Nudged to Observed Climatology

[18] Ocean models are prone to bias and drift because of, for example, inadequate resolution and poor boundary conditions. We use a technique developed by *Thompson et al.*

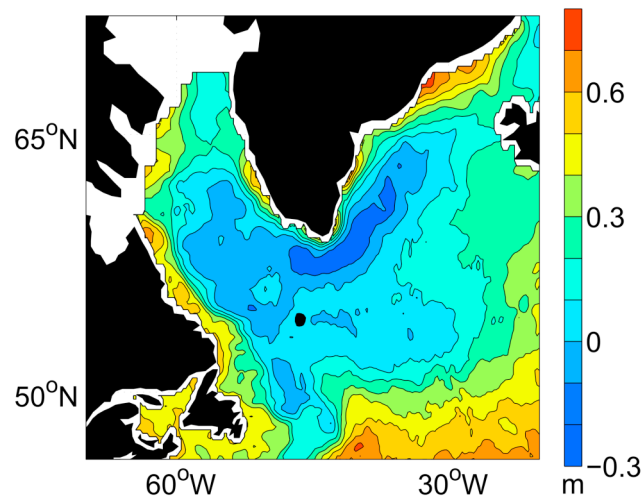


Figure 3. Mean sea surface topography derived from satellite and terrestrial gravity data (MSST_G). Areas within $\frac{1}{4}^\circ$ of the coastline are excluded.

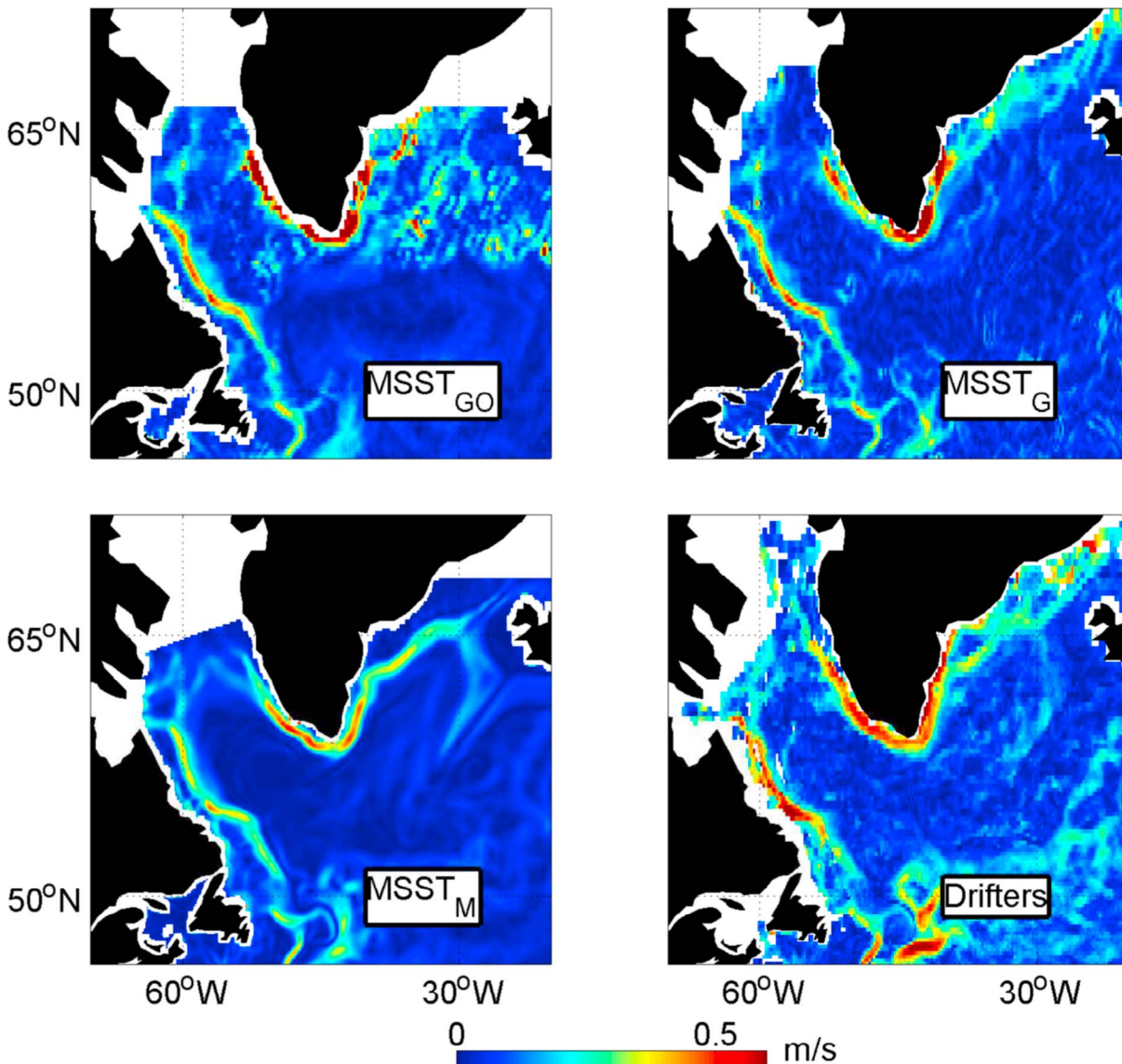


Figure 4. Speed of the mean surface geostrophic flow derived from $MSST_{GO}$, $MSST_G$, $MSST_M$, and drifters. (top left) Speed derived from the spatial gradients of $MSST_{GO}$, a geodetic estimate of the topography from *Thompson et al.* [2009]. (top right) Speed estimated using $MSST_G$, the geodetic estimate of topography described in this study. (bottom left) Same as for the top right plot but from $MSST_M$, produced by an ocean model spectrally nudged to a new Argo period TS climatology. (bottom right) Speed based on Global Drifter Program observations adjusted for Ekman drift.

[2006] which reduces bias and drift by nudging the model toward TS climatological values in prescribed frequency–wave number bands (see below for details). They refer to this technique as spectral nudging.

[19] Existing climatologies, such as the global $\frac{1}{4}^\circ$ World Ocean Atlas 2001 climatology [*Boyer et al.*, 2005] and the North Atlantic climatology of [*Lozier et al.*, 1995], are based on observations collected over many decades. Variability on interannual and decadal time scales may result in a climatology that does not correctly reflect conditions over a shorter time period. Here we use instead a monthly TS climatology that we construct using data collected by the Argo network over a 10 year period.

[20] The Argo network aims to maintain a global array of approximately 3000 drifting profilers. The floats cycle to a depth of 2000 m every 10 days, sending the resulting TS measurements to data centers via the Global Telecommunications System in near real time. The first floats were deployed in 2000, with full deployment in 2007, achieving the target average distribution of 3° spacing and measuring approximately 100,000 profiles each year. To reduce aliasing of mesoscale variability, we use the method of [*Higginson et al.*, 2009] whereby the Argo TS profiles are deduced using satellite altimeter sea surface height anomalies. This method uses only the altimeter anomalies and Argo TS measurements and requires no prior knowledge

of the mean. The deeded Argo TS profiles are mapped to monthly $\frac{1}{4}^\circ$ grids corresponding to the model grid using an optimal interpolation scheme with a background based primarily on the World Ocean Atlas 2005 (WOA05) [Antonov *et al.*, 2006; Locarnini *et al.*, 2006].

[21] The ocean model is based on version 2.3 of Nucleus for European Modelling of the Ocean (NEMO) with the Océan Parallélisé (OPA) ocean component [Madec *et al.*, 1998] and Lovain-la-Neuve Sea Ice Model (LIM) sea ice component [Fichefet and Maqueda, 1997]. The model grid is a North Atlantic subset (5°N – 68°N , 100°W – 34°E) of a global tripolar grid with nominal $\frac{1}{4}^\circ$ resolution and a maximum of 46 levels in the vertical. The surface forcing is the Coordinated Ocean Research Experiments (CORE) normal year data set [Large and Yeager, 2009] and temperature, salinity, and transport are prescribed at the open boundaries from a global $\frac{1}{4}^\circ$ model. To suppress model biases in temperature and salinity, the model has been spectrally nudged [Thompson *et al.*, 2006]. The basic idea of this technique is to nudge the model's climatology toward an observed climatology in selected wave number and frequency bands (in this case the climatologically important frequencies of 0 and 1 cycles per year). Outside of these frequency bands the model state is not nudged and can evolve prognostically. For more details on the technique and its implementation see Wright *et al.* [2006] and Stacey *et al.* [2006]. The model is used to produce a time–mean sea surface topography (MSST_M) and associated mean surface geostrophic velocities. Total speed derived from MSST_M is shown in Figure 4 (bottom left).

[22] The Argo data used to construct the TS climatology have no noticeable seasonal bias related to winter ice coverage. This is not surprising because the floats operate in waters deeper than 2000 m which, around southern Greenland and Labrador, are generally ice free.

3.2. Near-Surface Drifter Trajectories

[23] The Global Drifter Program is an array of satellite-tracked surface-drifting buoys designed to provide observations of mixed layer currents and sea surface temperature [Lumpkin and Pazos, 2007]. The first large-scale deployments occurred in 1988, and the array achieved the target of 1250 drifters (an average 5° spacing) in 2005. The buoys are of various designs but mostly comprise a surface float attached to a drogue at 15 m depth. Data are transmitted via the ARGOS satellite system, with the drifter position inferred from the Doppler shift of its transmission as the satellite passes over. The data are quality controlled by the Drifter Data Assembly Center and are interpolated to a regular $\frac{1}{4}$ day interval.

[24] For this study we analyze all drifter observations from 1991 to 2009. Drifters that have lost their drogue experience a greatly increased slip, and we exclude such drifters from this analysis. The remaining observations are adjusted for Ekman drift using the technique of Niiler and Paduan [1995] and wind data from the National Centers for Environmental Prediction–National Center for Atmospheric Research (NCEP–NCAR) reanalysis project [Kalnay *et al.*, 1996]. The adjusted velocities are then binned and averaged on a $\frac{1}{4}^\circ$ grid (Figure 4, bottom right). It should be noted that the adjustment technique of Niiler and Paduan [1995] is based on observations in the northeast Pacific Ocean, and extrapolating

this approach to the subpolar Atlantic may reduce the accuracy of the Ekman correction.

[25] We also analyzed drifter observations from 2000 to 2009, corresponding to the Argo period, using a similar technique. The standard error of observations within individual bins is higher for this reduced data set. Allowing for this increased uncertainty, the resulting circulation was broadly similar to the full data set but with less complete coverage of critical regions. Accordingly, we will discuss the full data set for the remainder of this paper.

3.3. Regional Mooring and Ship-Based Observations

[26] There have been a number of recent regional studies which describe velocity observations made within the subpolar gyre. These include Sutherland and Pickart [2008] (the East Greenland Current and East Greenland Coastal Current), Fratantoni and Pickart [2007] (the West Greenland Current and Labrador Current), Myers *et al.* [2009] (the West Greenland Current), and Bacon *et al.* [2008] (the East and West Greenland Currents and the Labrador Current). While observations from these studies are biased toward the summer months and mostly relate to short time periods, they are useful for validating drifter observations, and they are discussed in section 4.

4. Evaluation of the New Geodetic Estimate

[27] The mean surface circulation derived from MSST_G (Figure 4, top right) shows relatively fast narrow currents along the coasts of Greenland and Labrador. The circulation from MSST_M (Figure 4, bottom left) and from the surface drifters (Figure 4, bottom right) show similar patterns. In each case the current around the south of Greenland is close to the coastline, reflecting the narrow shelf in this region. The path of the Labrador Current is similar in each and follows the shelf break. The current follows the edge of the Grand Banks off of Newfoundland, with the North Atlantic Current entering the domain from the south at about 45°W . The current speeds are broadly similar for the MSST_G and MSST_M plots, but the drifter speed estimates appear to be a little higher. In order to provide a more detailed and quantitative comparison, we examine a number of smaller regions which are identified in Figure 5.

4.1. East Greenland Current

[28] The East Greenland Current extends from the northeast of Greenland southward along the coast to Cape Farewell [Bacon *et al.*, 2008], but here we consider only the current south of Denmark Strait. The surface circulation is believed to comprise the main East Greenland Current (EGC) following the shelf break, with the Irminger Current (IC) alongside but farther offshore, and a narrower current (the East Greenland Coastal Current (EGCC)) on the shelf closer to shore [Sutherland and Pickart, 2008]. The IC carries high-salinity Atlantic-origin waters, whereas the EGC and EGCC contain low-salinity Arctic-origin waters. Sutherland and Pickart [2008] examined six transects across the shelf occupied during the summer of 2004, together with other transects from 2002 and 2003. They identified the EGCC as a narrow (20–40 km wide) current on the shelf with speeds in the range 0.5 – 1 m s^{-1} . These transects show that the EGC follows the shelf edge with speeds in the range 0.1 – 0.5 m s^{-1} . They

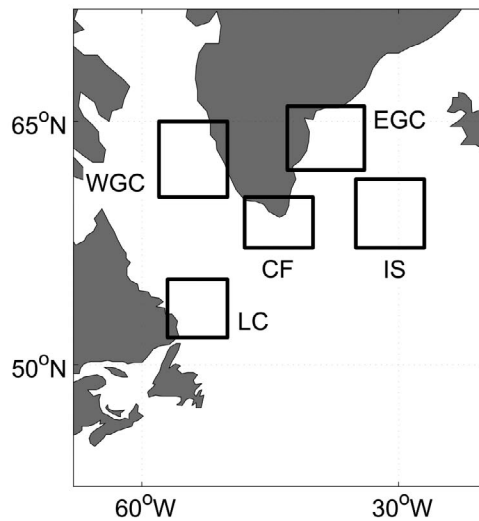


Figure 5. Locations of the subregions examined in section 4: East Greenland Current (EGC), Cape Farewell (CF), West Greenland Current (WGC), Labrador Current (LC), and Irminger Sea (IS).

suggest that the EGCC is an inner branch of the EGC controlled by bathymetric steering, whereas *Bacon et al.* [2008] propose that it is a separate current formed mainly from sea ice melt.

[29] To examine the strengths and weaknesses of $MSST_G$, we consider part of the East Greenland Current, the region labeled EGC in Figure 5. Plots of current velocity vectors for each of the data sets are shown in Figure 6. Figure 6 (top right) shows the mean surface currents estimated from drifters, and this is in broad agreement with recent descriptions of the current system [e.g., *Sutherland and Pickart, 2008*]. Two currents can be identified, the EGC following the shelf edge (shown in Figure 6 (top right) by the 700 m isobath) and the EGCC on the shelf much closer to shore. The two currents come together around 63°N where the shelf narrows, although other plots (not shown here) reveal that the currents separate again farther to the south. The EGCC reaches speeds in excess of 0.5 m s^{-1} , and the EGC is somewhat slower and broader. Figure 6 (top left) shows velocities derived from $MSST_G$, and this shows a similar overall pattern. There is good agreement of current speed and position south of 63°N. To the north both currents are slower than the drifter estimates, and the EGCC is located farther from shore. This may

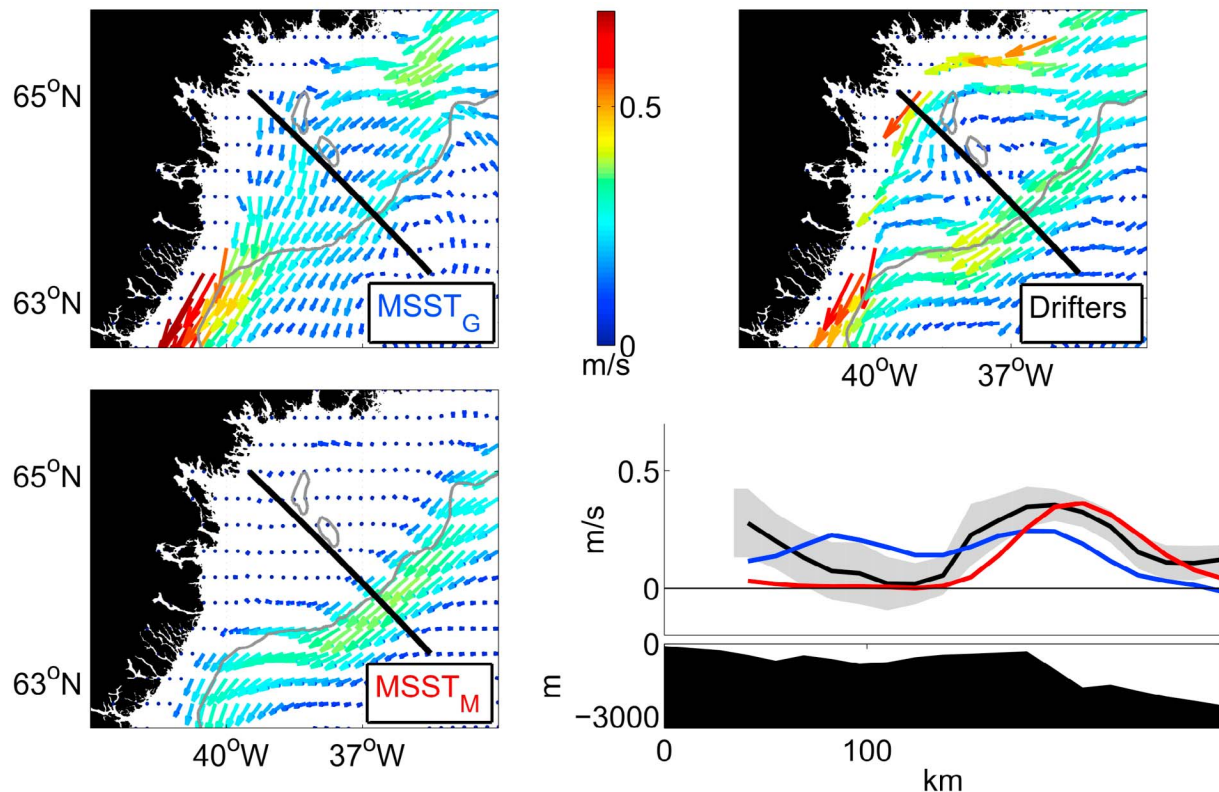


Figure 6. Estimates of the mean surface geostrophic flow for part of the East Greenland Current (62.5°N–65.75°N, 43°W–34°W, labeled EGC in Figure 5). Velocity vectors derived from the spatial gradients of (top left) $MSST_G$ and (bottom left) $MSST_M$ and from (top right) surface drifter observations. Vector size and color are related to speed. The black line shows the position of the section plotted in the bottom right plot, and the grey line is the 700 m isobath, representative of the shelf edge. (bottom right) Mean surface current speed normal to the section plotted on the previous plots derived from the gradients of $MSST_G$ (blue) and $MSST_M$ (red) and from the surface drifters (black). The grey shaded area is the error for the drifter estimate, calculated as 2 times the standard error of the sample mean. The bathymetry and distance from shore are plotted beneath.

Table 1. Comparisons of the Sea Surface Topographies $MSST_G$ and $MSST_{GO}$ With $MSST_M$ for Each of the Subdomains Described in Section 4^a

	$MSST_M$	$MSST_G$	$MSST_{GO}$	$MSST_M-MSST_G$	$MSST_M-MSST_{GO}$	$\rho_{M,G}$	$\rho_{M,GO}$
EGC	18.8	24.5	24.0	13.6	18.1	0.79	0.61
CF	22.3	24.8	27.8	8.1	11.9	0.92	0.91
WGC	17.7	18.6	21.3	10.3	14.2	0.82	0.73
LC	20.3	20.7	22.2	4.5	5.5	0.97	0.97
IS	8.8	5.6	12.0	4.7	8.0	0.89	0.74

^aThe first five columns show the standard deviation (cm) of all grid points within each subdomain for $MSST_M$, $MSST_G$, and $MSST_{GO}$ and their differences. The final two columns are the correlation between $MSST_M$ and $MSST_G$ and between $MSST_M$ and $MSST_{GO}$. The subdomains are shown in Figure 5. Subdomains are East Greenland Current (EGC), Cape Farewell (CF), West Greenland Current (WGC), Labrador Current (LC), and Irminger Sea (IS).

point to a weakness in the offshore gravity data in this area. Figure 6 (bottom left), derived from $MSST_M$, shows the EGC in very good agreement with the drifter estimates, but the EGCC is almost absent. Weak along-shelf flow is a known deficiency of this model configuration, possibly due to the poor resolution of the climatology on the shelf, poor boundary conditions, or inadequate atmospheric forcing. The cross-current section of Figure 6 (bottom right) illustrates the broad agreement between the three estimates for the position of the EGC and the differences for the EGCC noted above.

[30] To provide a quantitative comparison, we provide statistics for $MSST_G$, $MSST_{GO}$, and $MSST_M$ (Table 1). There is a reasonably high correlation between $MSST_M$ and $MSST_G$ ($\rho = 0.79$), but the standard deviation of the differences is also fairly high (13.6 cm). This is not surprising given the almost complete lack of the EGCC in $MSST_M$. $MSST_G$ is a considerable improvement over the earlier geodetic estimate, $MSST_{GO}$, described by *Thompson et al.* [2009]. The correlation between $MSST_{GO}$ and $MSST_M$ is 0.61, and the standard deviation of the differences is 18.1 cm, more than 30% higher than the corresponding figure for $MSST_G$.

[31] We similarly calculate statistics of comparison for the alongshore component of the speeds derived from $MSST_G$ and the drifter estimates (Table 2; see footnote for details of the alongshore direction). As expected, the correlation between the drifters and $MSST_G$ is lower ($\rho = 0.59$), and the standard deviation of the differences remains high (16.0 cm s⁻¹). However, $MSST_G$ is again shown to be an improvement over $MSST_{GO}$. The correlation between $MSST_{GO}$ and the drifters is 0.47, and the standard deviation of the differences is 18.3 cm s⁻¹.

[32] A small shift in the position of a current may result in poor statistics of comparison and, as noted previously, there is a difference in the position of the EGCC between $MSST_G$ and the drifters on the shelf around 65°N. There are few direct observations of the EGCC in this area, and there are large

uncertainties attached to the drifter estimates. *Sutherland and Pickart* [2008, section 3] include observations from summer 2004 close to 65°N, and they observe a jet between 25 and 30 km offshore. This is within the region close to shore where the geodetic technique is unable to accurately estimate MSST because of reduced accuracy of the satellite altimeter. On the other hand, their section does not extend out to the region where a jet is seen in the $MSST_G$ data, 80–100 km offshore. It is possible that $MSST_G$ is not observing the EGCC as defined by *Sutherland and Pickart* [2008] or that there is seasonality to the position of the current which they do not observe. This is an area for further study.

4.2. Cape Farewell

[33] *Holliday et al.* [2007] describe the circulation around Cape Farewell (the southernmost tip of Greenland) using data from a summer 2005 cruise. They find that the EGC and EGCC merge again into a single current where the shelf widens directly to the south of Cape Farewell, in agreement with drifter observations described by *Cuny et al.* [2002]. The combined flow turns toward the northwest to form the West Greenland Current (WGC) with a partial subsurface retro-reflection feeding a recirculation in the Irminger Sea. *Clarke* [1984] deployed current meters in the Irminger Current south of Cape Farewell for two months during the winter of 1978 and found subsurface (100 m depth) currents flowing approximately westward with mean speeds of about 0.3 m s⁻¹ near the shelf break and 0.15 m s⁻¹ over the slope.

[34] Figure 7 shows velocity plots for the Cape Farewell region. The drifter velocity estimate (Figure 7, top right) is in agreement with the description of *Holliday et al.* [2007]. The EGC and EGCC form a single current and follow the shelf break toward the northwest. The currents calculated from $MSST_G$ (Figure 7, top left) follow a similar pattern, and the merged current has a mean speed of about 0.6 m s⁻¹. This is in good agreement with the drifters described by *Cuny et al.*

Table 2. Statistics of Fit for the Alongshore Component of the Speeds Estimated From Drifters and From $MSST_G$ and $MSST_{GO}$ for Each of the Subdomains Described in Section 4^a

	Drifters	$MSST_G$	$MSST_{GO}$	Drifters- $MSST_G$	Drifters- $MSST_{GO}$	$\rho_{D,G}$	$\rho_{D,GO}$
EGC	24.2 (19.9)	17.9 (23.6)	10.1 (20.2)	4.6 (16.0)	7.3 (18.3)	0.59	0.47
CF	15.1 (17.7)	12.1 (20.4)	7.8 (18.9)	3.2 (9.8)	3.4 (10.8)	0.84	0.82
WGC	17.7 (17.3)	11.5 (15.3)	10.8 (26.1)	5.7 (13.4)	5.6 (18.0)	0.66	0.73
LC	19.1 (18.4)	10.9 (17.1)	13.1 (12.4)	6.8 (11.0)	5.6 (11.8)	0.81	0.77
IS ^b	7.5 (9.6)	1.2 (2.9)	2.5 (8.3)	6.0 (10.5)	4.5 (13.4)	0.20	0.12

^aThe first five columns show the mean and standard deviation (cm s⁻¹) of alongshore speed at all grid points within each subdomain for drifters, $MSST_G$, and $MSST_{GO}$ and for their differences. Standard deviations are shown in parentheses. The final two columns are the correlations of alongshore speed between drifters and $MSST_G$ and between drifters and $MSST_{GO}$. The subdomains are shown in Figure 5. Alongshore is defined as a bearing of 225° for East Greenland Current (EGC), 270° for Cape Farewell (CF), 330° for West Greenland Current (WGC), and 150° for Labrador Current (LC).

^bFor Irminger Sea (IS), which is open ocean, we show the statistics for zonal flow.

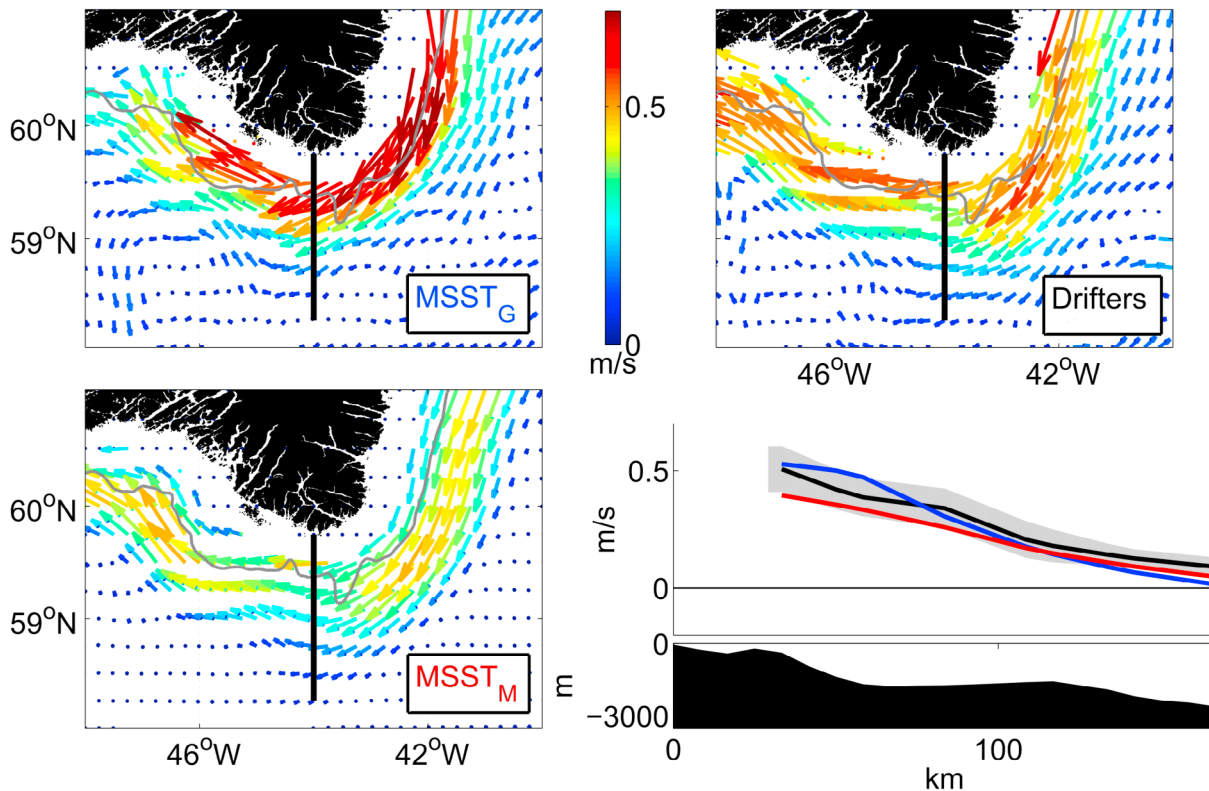


Figure 7. Same as for Figure 6 but for the Cape Farewell region (58°N–61°N, 48°W–40°W, labeled CF in Figure 5).

[2002], which ranged between 0.3 and 0.9 m s⁻¹ over the shelf, and were a little faster than the subsurface measurements by *Clarke* [1984]. The currents derived from MSST_M (Figure 7, bottom left) follow a similar pattern, but speeds are lower, especially on the shelf. The section plot (Figure 7, bottom right) shows good agreement south of Cape Farewell for all three estimates of the along-shelf current speed and position.

[35] The statistics of comparison for MSST_G and MSST_M (Table 1) show a high correlation ($\rho = 0.92$), and the standard deviation of the differences between the two fields (8.1 cm) is much lower than for the individual fields. Unlike the East Greenland Current region, MSST_G in this region is only a small improvement over the earlier geodetic estimate, MSST_{GO}. The correlation between MSST_{GO} and MSST_M is almost the same ($\rho = 0.91$), but the standard deviation of the differences is somewhat higher (11.9 cm).

[36] Similarly, statistics of comparison of the alongshore velocity components from MSST_G and from the drifters (Table 2) show a high correlation ($\rho = 0.84$). There is only a small improvement in both correlation and standard deviation of the differences compared with MSST_{GO}.

4.3. West Greenland Current

[37] The West Greenland Current extends from Cape Farewell northward along the west coast of Greenland. The current transports cold, fresh waters along the shelf and warmer, saltier waters (of Irminger Current origin) over the slope, with the strongest velocities over the shelf break [*Fratantoni and Pickart*, 2007]. There are few direct mea-

surements of the current's velocity [*Myers et al.*, 2009], but drifter estimates include 0.7 m s⁻¹ near Cape Farewell decreasing to 0.4 m s⁻¹ near Fylla Bank [*Krauss*, 1995] and maxima of 0.95 m s⁻¹ near Cape Farewell decreasing northward to 0.7 m s⁻¹ and a mean velocity of 0.35 m s⁻¹ [*Cuny et al.*, 2002]. *Fratantoni and Pickart* [2007] estimate a mean summer velocity in excess of 0.3 m s⁻¹ using TS observations and a thermal wind calculation. *Myers et al.* [2009] use an ocean model spectrally nudged to a TS climatology and estimate mean velocities decreasing from 0.3 m s⁻¹ near Cape Farewell to 0.15 m s⁻¹ off Fylla Bank. The current bifurcates with two branches turning to the west, approximately following the 1500 and 3000 m isobaths, and the remnant West Greenland Current continuing northward toward Davis Strait [*Cuny et al.*, 2002].

[38] Figure 8 shows velocity plots for part of the West Greenland Current in the vicinity of Fylla Bank. The drifter velocity estimate (Figure 8, top right) shows a pattern similar to descriptions by, for example, *Cuny et al.* [2002] and *Fratantoni and Pickart* [2007]. The main West Greenland Current follows the shelf break, shown on these plots by the 700 m isobath, with mean speeds in the range 0.4–0.6 m s⁻¹. Bifurcation of the main jet can be identified, with branches of the current turning to the west approximately following the 3000 and 1500 m isobaths but somewhat slower than the coastal current.

[39] The velocity field derived from MSST_G shows a similar path and speed for the shelf break current, although north of 64°N the current is much slower than the drifter estimate. This may be related to the seasonality of the drifter

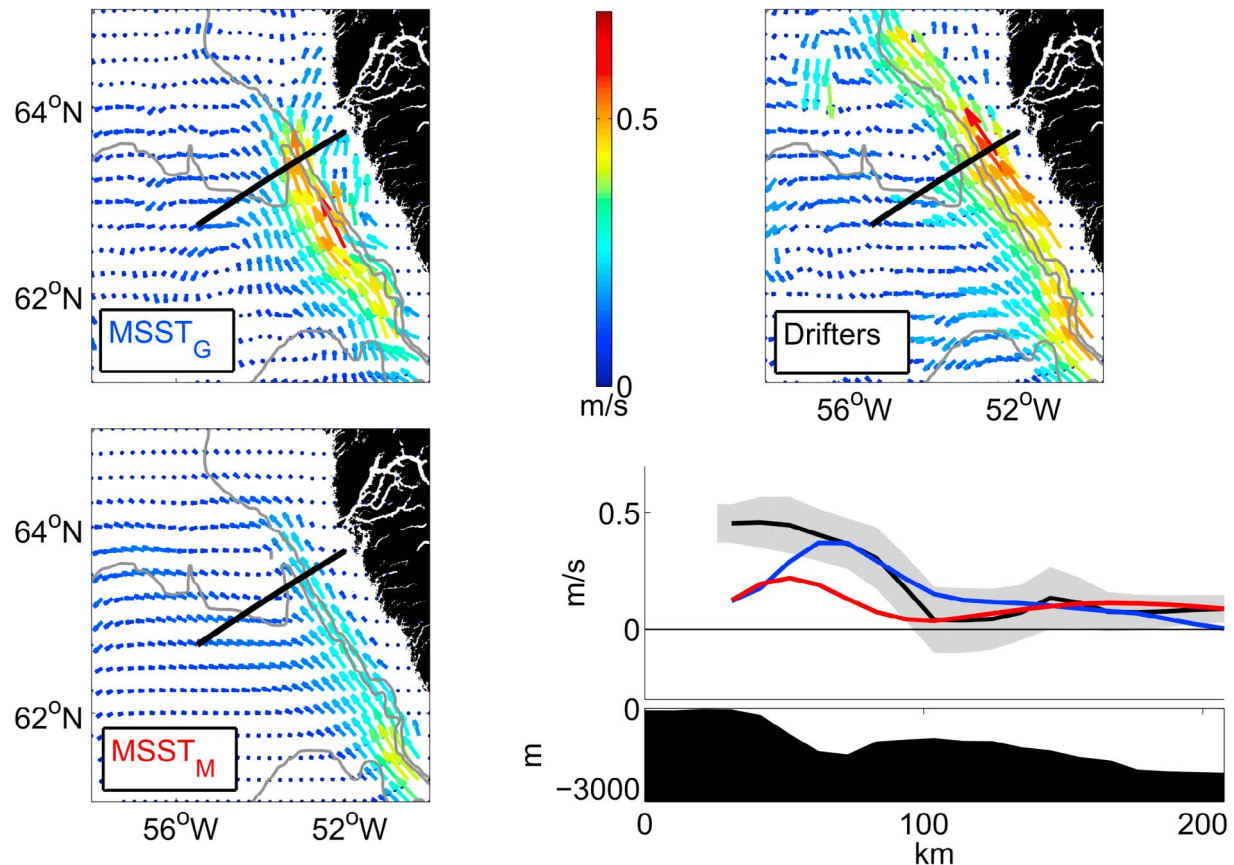


Figure 8. Same as for Figure 6 but for part of the West Greenland Current (61°N – 65°N , 58°W – 50°W , labeled WGC in Figure 5). The grey lines are the 700, 1500, and 3000 m isobaths.

observations since the drifter speed estimate is derived from just 13 floats, 10 of which passed through the region during the ice-free months of July to December. There is no sign of a bifurcation at the 3000 m isobath on the MSST_G plot, but there is a weak branch of the current following the 1500 m isobath. The speeds derived from MSST_M are generally somewhat less than the other estimates, although the main current still follows the shelf break. The flow almost disappears north of 64°N , and flow on the shelf is very weak. The 1500 m bifurcation can be identified, although the current speed is somewhat less than the drifter estimate. The section (Figure 8, bottom right) cuts across Fylla Bank, showing the main shelf break current and 1500 m isobath branch in the drifter speed estimates. There is reasonable agreement with the speeds from MSST_G , but the coastal current estimated from MSST_M is too weak.

[40] With broad agreement on the position and strength of the WGC, the correlation between MSST_G and MSST_M is quite high (Table 1, $\rho = 0.82$). The standard deviation of the differences (10.3 cm) is much lower than the standard deviation of either MSST_G or MSST_M . These values are a significant improvement over the statistics comparing MSST_{GO} and MSST_M ($\rho = 0.73$ and standard deviation of differences is 14.2 cm).

[41] The correlation between MSST_G and the drifters is somewhat lower (Table 2, $\rho = 0.66$), and the standard deviation of the differences remains high (13.4 cm s^{-1}). This is, at

least partly, due to the relative strength of the bifurcation flows and the WGC north of 64°N in the drifter estimate. (For example, the correlation is higher when the area north of 64°N is excluded.) There are few observations in this region, but it is interesting that an analysis of surface drifters by *Cuny et al.* [2002, Figure 4b] shows a surface circulation very similar to the MSST_G estimate. Their analysis indicates a rapid slowing of the WGC around 64°N and bifurcation speeds mostly 10 cm s^{-1} or less. It is possible that the drifter analysis, based on a small number of observations, has overestimated the current speed in some areas and that MSST_G is a better representation of the mean circulation.

4.4. Labrador Current

[42] Flow from the West Greenland Current turns to the south as it reaches the Labrador shelf, joining waters exiting Davis Strait and Hudson Strait to form the Labrador Current [Loder et al., 1998]. The current continues southward as far as the Grand Banks, bifurcating at the Tail of the Banks with part of the flow continuing southward and part joining the North Atlantic Current.

[43] The Labrador Current has been the subject of more intensive observation than the East and West Greenland Currents. For example, *Lazier and Wright* [1993] describe the structure and seasonality of the current around Hamilton Bank using data collected over 10 years from oceanographic sections and moorings. They describe the main current

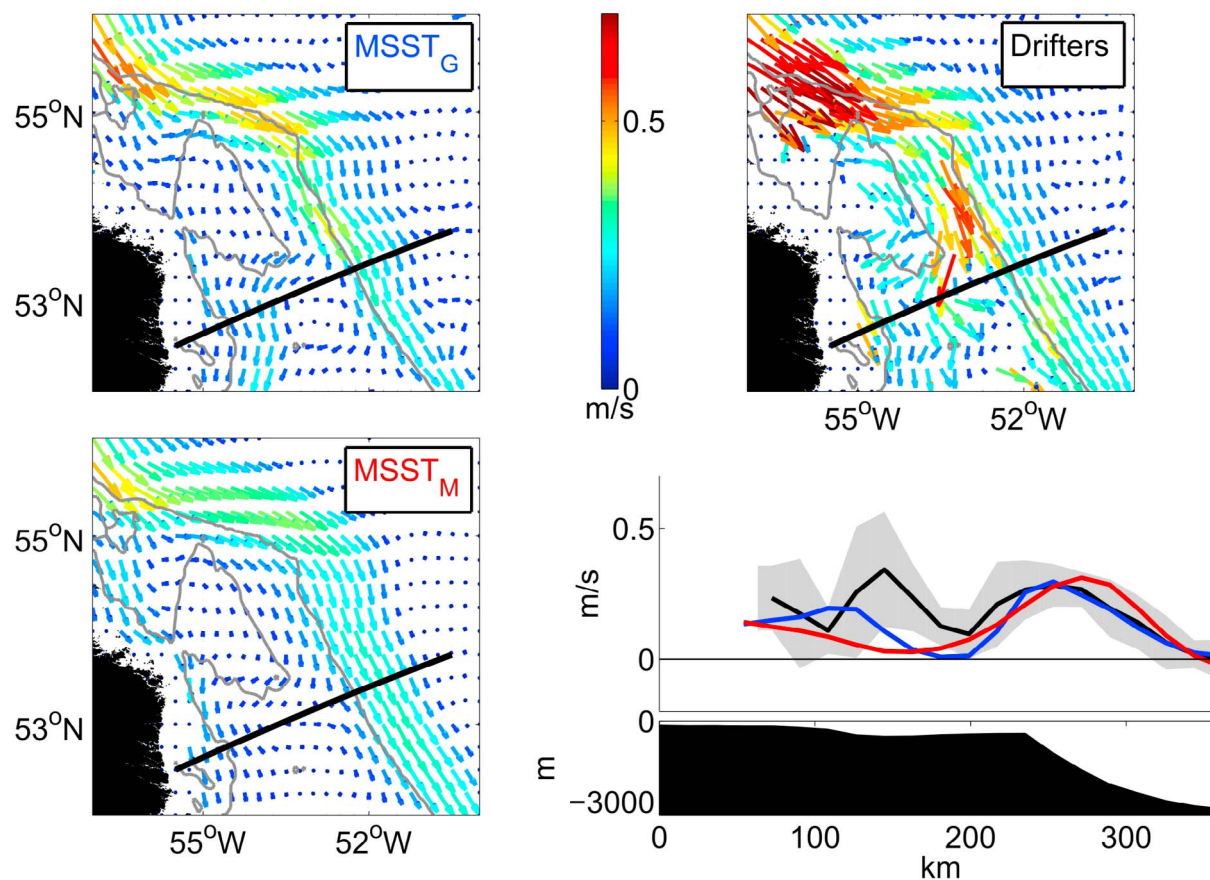


Figure 9. Same as for Figure 6 but for part of the Labrador Current (52°N–56°N, 57°W–50°W, labeled LC in Figure 5). The grey lines are the 200 and 700 m isobaths. Hamilton Bank is the shallow area centered near 54°N, 55°W.

located over the shelf break, with a maximum surface speed of 0.28 m s^{-1} , and a smaller inshore branch of the current, located over the shelf between Hamilton Bank and the coastline, peaking at 0.12 m s^{-1} . Colbourne *et al.* [1997] calculate a speed in excess of 0.3 m s^{-1} relative to flow at 500 m depth for the shelf break current near Hamilton Bank using TS data collected over more than 40 years and a speed of less than 0.1 m s^{-1} for the inshore branch. Lazier and Wright [1993] observe seasonality to the current velocity, with a maximum in October and a minimum around March and April.

[44] Figure 9 shows velocity plots for the region around Hamilton Bank. The plot derived from MSST_G (Figure 9, top left) shows the main shelf break current with mean speeds in the range $0.3\text{--}0.6 \text{ m s}^{-1}$ and branches flowing onto the shelf on either side of Hamilton Bank with speeds of $0.1\text{--}0.3 \text{ m s}^{-1}$. The structure of the currents and the speeds are in good agreement with the drifter estimates (Figure 9, top right), although the drifter speeds are a little higher in places. There is good agreement for flow onto the shelf south of Hamilton Bank, but the drifter data set includes insufficient measurements to estimate velocities in the shallow water between the bank and the coast. The currents derived from MSST_M show a similar structure, although speeds are generally lower. The cross-current section, which is just to the south of Hamilton

Bank, shows good agreement between all three estimates for the position and speed of the main shelf break current.

[45] Correlation between MSST_G and MSST_M is high (Table 1, $\rho = 0.97$), and the standard deviation of the differences is low (4.5 cm). This correlation is identical to that between MSST_{GO} and MSST_M, which is to be expected since the geoid used by Thompson *et al.* [2009] incorporates much the same gravity data for this region as the new geoid. Similarly, statistics comparing MSST_G and the drifters (Table 2) show that the correlation is fairly high ($\rho = 0.81$), and this is only a slight improvement over MSST_{GO} ($\rho = 0.77$).

[46] Bacon *et al.* [2008] suggest that the current on the shelf exists as a separate current system rather than a branch of the main Labrador Current, possibly originating with coastal meltwaters. However, all of our estimates show flow onto the shelf near 55°N and again near 54°N, indicating that the coastal current is at least partially formed from Labrador Current waters.

4.5. Irminger Sea

[47] For completeness we also include statistics of comparison for an area of open ocean within the Irminger Sea. This region was noted by Thompson *et al.* [2009] as one of the areas where their MSST contains spurious features because of poor gravity data in the geoid model.

[48] Correlation between $MSST_G$ and $MSST_M$ is high (Table 1, $\rho = 0.89$) and a significant improvement over $MSST_{GO}$ ($\rho = 0.74$). The standard deviation of the differences is reduced from 8.0 cm for $MSST_{GO}$ to 4.7 cm for $MSST_G$. The correlation between $MSST_G$ and drifters is much lower (Table 2, $\rho = 0.20$), albeit an improvement over $MSST_{GO}$ ($\rho = 0.12$). This is a region of low current speeds, but the drifter estimate has high variability, and this may account for the low correlation. $MSST_{GO}$ includes many erroneous circulation features which do not appear in $MSST_G$. The standard deviation of the zonal current estimates from $MSST_G$ is 2.9 cm s^{-1} , significantly less than the corresponding figure for $MSST_{GO}$ (8.3 cm s^{-1}).

5. Discussion

[49] This study uses two techniques to produce estimates of the mean sea surface topography of the subpolar gyre. First, we extend the work of *Thompson et al.* [2009], who used satellite and terrestrial gravity measurements to produce good estimates of the Gulf Stream and Labrador Current. However, there were spurious circulation features around Greenland, caused, for example, by high wave number variability in the geoid south of Iceland, and the narrow coastal currents around Greenland were poorly resolved.

[50] This study uses improved gravity data and improved quality control. A visual comparison of the velocity estimates from the new mean sea surface topography ($MSST_G$) and those obtained from surface drifters and oceanographic observations indicates good agreement. The main features of the subpolar gyre surface circulation are apparent, and the current speeds are generally consistent with other estimates. The $MSST$ is much improved around Greenland. The spurious circulation features apparent in the earlier work are no longer present, and the resolution of the coastal currents is improved, including the narrow (20–40 km wide) East Greenland Coastal Current.

[51] A quantitative comparison of the old [*Thompson et al.*, 2009] and new geodetic topographies shows small improvements in the correlation of the geodetic topography with the model estimate in the Labrador Current, as expected given the minor changes to the gravity data in this region. Much larger improvements are seen around Greenland, where the gravity data were revised more extensively. For example, the correlation between $MSST_G$ and drifters for alongshore currents in the East Greenland Current region shown in Figure 5 increases from 0.47 for the old topography to 0.59. In the West Greenland Current the standard deviation of the differences between the new geodetic estimates of alongshore velocity and the drifter estimate is reduced by more than 25% compared with the *Thompson et al.* [2009] estimate.

[52] Second, we produce an estimate of the $MSST$ using an ocean model spectrally nudged to a new Argo period TS climatology. Comparison of velocities derived from $MSST_G$ and from the ocean model ($MSST_M$) shows broad agreement in deeper waters over the shelf slope. However, there is frequently poor agreement in shallow water on the shelf, with $MSST_G$ in closer agreement with drifter and other estimates. This may be because the climatology used to nudge the model incorporates Argo data but defaults to the relatively low resolution WOA05 climatology in shallow water where Argo does not operate.

[53] One of the attractions of using these techniques to study the circulation is the possibility of obtaining multiyear mean values across a large geographic area. The altimeter and drifter measurements used in this study are subject to a seasonal observation bias (see Appendix B), which may lead to a bias in the mean circulation estimates. However, we have repeated the quantitative comparison of the topographies using data restricted to the ice-free seasons, and it does not seem to significantly alter the results for the scales and relatively short data record examined here.

[54] An interesting observation from these results is that $MSST_G$ shows flow between the main Labrador Current and the coastal current. This indicates that the coastal current is, at least in part, formed as a branch of the main current rather than being of separate origin. A similar possibility arises with the East Greenland Current. There is some indication of flow between the main current and the coastal current in the estimate from $MSST_G$, but it is a little less clear than for the Labrador Current. This may be the result of a weakness in the terrestrial gravity data or the nearshore altimeter data.

[55] In conclusion, this study provides further evidence that a geodetic approach using both GRACE and terrestrial gravity data provides a realistic estimate of the mean sea surface topography. The resulting mean surface circulation speed estimates are comparable with in situ measurements, and relatively small circulation features such as the East Greenland Coastal Current are resolved. The circulation close to shore may be improved by future improvements in the processing of altimeter data in the coastal zone. New gravity data will be available soon from the Gravity Field and Steady-State Ocean Circulation Explorer (GOCE) satellite mission, and this should also lead to improvements in the accuracy of the geoid and the large-scale circulation estimates in future work. It is likely, however, that terrestrial gravity data will still be required to resolve the smaller-scale circulation features.

Appendix A: The PCG08I Geoid Model

[56] The marine gravity field of PCG08I is defined on a 2 min by 2 min grid. It makes use of shipboard gravity data, six gravity models derived from satellite altimetry, and the Arctic Gravity Project 2008 (ArcGP08) data set (http://earth-info.nga.mil/GandG/wgs84/agp/readme_new.html). The six altimetry-derived gravity models are GSFC00 [*Wang*, 2001], CLS01 (CLS, France), NTCU01 [*Hwang et al.*, 2002], KMS02 [*Andersen et al.*, 2005], DNSC08 [*Andersen et al.*, 2010], and Sandwell and Smith v9 [*Sandwell and Smith*, 2009].

[57] The realization of the marine gravity grid for PCG08I follows a multistep approach. As a criterion each step fills only grid nodes that are undefined; that is, the nodes filled by preceding steps retain their values at each step. The whole approach consists of seven steps:

[58] 1. The shipboard gravity data are compared to each altimetry-derived gravity model. If the difference at a node is 2 mGal or less, then the two values are averaged and the mean value is used.

[59] 2. The gaps along the Atlantic coast of Canada (Labrador, Newfoundland, and Nova Scotia) are filled with the dense shipboard gravity data set.

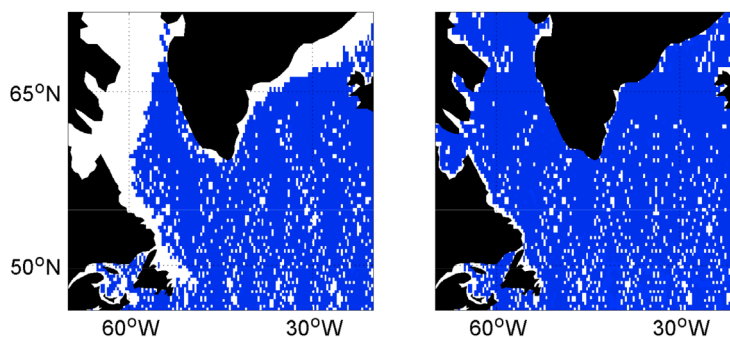


Figure B1. Altimeter measurements of sea level anomalies during the months of (left) April 2008 and (right) October 2008. The blue areas represent the availability of altimeter along-track measurements by the Jason 1, Jason 2, and Envisat missions in the processed data sets distributed by Aviso.

[60] 3. The eight gravity data sets (shipboard, six altimetry-derived models, and ArcGP08) are averaged, and the mean is used if the range of the eight data are equal to or less than 5 mGal.

[61] 4. The three data sets (shipboard, ArcGP08, and DNSC08) covering most of the Arctic region are averaged when the data range is equal to or less than 5 mGal.

[62] 5. The six altimetry-derived grids are averaged, and the mean is kept if the range of the six values at a node is within 3 mGal.

[63] 6. The mean value between ArcGP08 and DNSC08 is used in the gravity grid if the difference is equal to or less than 5 mGal.

[64] 7. Finally, the remaining undefined nodes over the oceans are determined from the DNSC08 altimetry-derived gravity model.

[65] The resulting model is a comprehensive combination of different mean gravity values. For the coast of Labrador, the gravity data are either mean values between shipboard data and altimetry-derived gravity data or shipboard data. For the coast of Greenland, the gravity nodes are not only mean values between shipboard data, altimetry-derived gravity data, and ArcGP08, but also, in large portion, DNSC08 gravity data. The previous grid [Thompson *et al.*, 2009] used ArcGP03 over and around Greenland, shipboard data along the Canadian east coast, and GSFC00 over vast unfilled ocean areas.

[66] The geoid model is computed using the same methodology as described by Thompson *et al.* [2009]. EGM08 [Pavlis *et al.*, 2008] is truncated to spherical harmonic degree and order 360 and combined with the PCG08I gravity grid to realize the 2 min by 2 min resolution geoid model. The computational process makes use of the remove-restore approach with a degree 90 modified degree-banded Stokes kernel [Huang *et al.*, 2007]. The low-degree part of EGM08 (degree 2 to degree 90) is dominated by the GRACE data. Thus, the resulting PCG08I model is defined on the GRACE gravity field for the low-degree components.

[67] The geoid error is the combination of the EGM08 commission error and terrestrial gravity data error. The EGM08 commission error estimated from its error coefficients is approximate because the full covariance matrix of the coefficient is not publicly available. The error of low-degree components (<90) of geoid model is less than 3 cm,

while the error of high-degree components (>90) of EGM08, which affect the geoid model through the far-zone contribution, is about 0.4 cm. The terrestrial gravity data contribute the largest error source in the realization of the PCG08I model. The errors range from a few centimeters to decimeters. The total geoid error is mostly between 1 and 5 cm for the study area. The approach for estimating geoid error is described by Huang *et al.* [2007].

Appendix B: Seasonality of Observations

[68] Most observations of the circulation of the subpolar gyre were made during the summer months when there is little or no ice coverage. Where observations have been year-round, seasonal variations in current speed have been observed. For example, Lazier and Wright [1993] observed seasonal variability in the Labrador Current with a maximum in October and a minimum in April. The alongshore surface current speed varies by a factor of 2 between the minima and maxima, and they speculate that this is caused by buoyancy forcing with ice melt and river runoff contributing fresh water to the system during the spring and summer. It is possible that the current descriptions of the circulation, being largely based on summer observations, incorporate a seasonal bias.

[69] MSST_G is intended to represent the mean field, but it is derived from the mean sea surface and there is a bias to the altimeter measurements from which this is constructed. Satellite altimeters are unable to measure sea surface height where there is old, multiyear ice, and so there will be fewer measurements in areas of sea ice than in ice-free areas. A plot of all altimeter tracks for the months of April and October 2008 (Figure B1) shows measurement-free areas along the east coast of Greenland and Labrador during April, corresponding with the typical extent of sea ice.

[70] The validation data sets, MSST_M and the surface drifters, are similarly intended to represent the mean annual circulation. MSST_M is produced using a TS climatology derived from Argo float measurements. Since these floats are restricted to the (largely) ice-free waters deeper than 2000 m, seasonal ice should not be an issue, although the background may include an inherent bias. Plots of the observation density of the surface drifters (Figure B2) show there to be fewer drifters on the ice-prone East Greenland and Labrador shelves during the winter months.

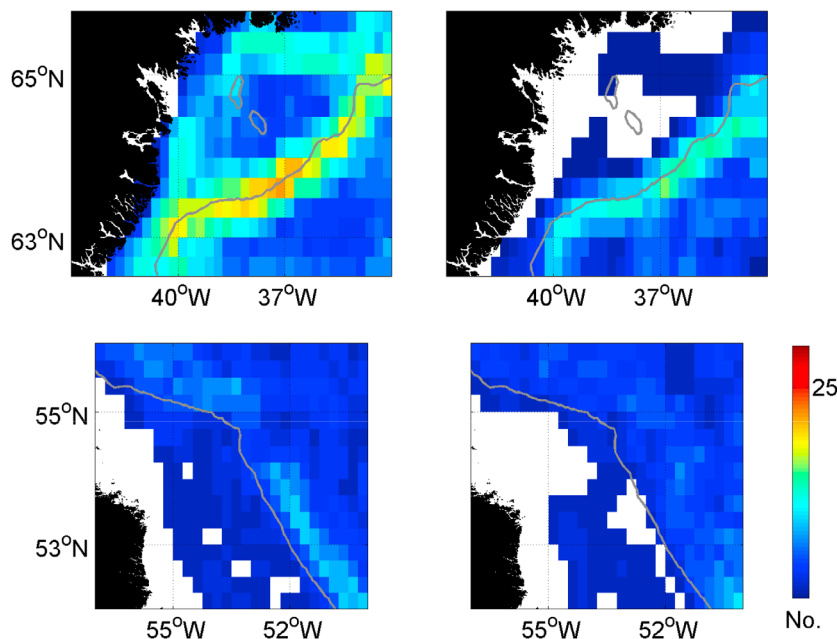


Figure B2. Observation density of the drifter data set by season. Total number of valid drifter observations, in $1/4^\circ$ bins, for the (top) EGC region and (bottom) LC region for (left) July to December inclusive and (right) January to June inclusive. The grey line in each plot indicates the 700 m isobath, representative of the shelf edge.

[71] We have repeated the quantitative comparison of each of the topographies and the resulting estimates of surface circulation using only data from the ice-free season, and this shows little change to the results. Although there may be a seasonal bias in data contributing to $MSST_G$, $MSST_M$, and the drifter estimates, it seems that, at the scales considered in this study, seasonality is not an issue. For future work at finer resolution this may become a concern, particularly for studies of the coastal currents on the shelves where ice forms.

[72] **Acknowledgments.** We acknowledge support from the GOAPP research network, and K.R.T. acknowledges support from the NSERC discovery grant program. The altimeter products were produced by Ssalto/Duacs and were distributed by Aviso, with support from CNES (<http://www.aviso.oceanobs.com/duacs/>). MSS_CNES_CLS10 was produced by CLS Space Oceanography Division and was distributed by Aviso, with support from CNES (<http://www.aviso.oceanobs.com/>). The Argo data were collected and made freely available by the International Argo Project and the national programs that contribute to it (<http://www.argo.ucsd.edu>, <http://argo.jcommops.org>). Argo is a pilot program of the Global Ocean Observing System. The NCEP reanalysis data were provided by the PSD, ESRL, OAR, NOAA, Boulder, Colorado, United States, from their Web site at <http://www.esrl.noaa.gov/psd/>. We would like to thank Zeliang Wang for providing the ocean model results and Yimin Liu for help with the Argo TS climatology. Finally, we would like to thank Allyn Clarke for his helpful comments on an earlier draft of this manuscript.

References

- Andersen, O., P. Knudsen, and R. Trimmer (2005), Improved high resolution altimetric gravity field mapping (the KMS2002 global marine gravity field), in *A Window on the Future of Geodesy*, *Int. Assoc. Geod. Symp.*, vol. 128, edited by F. Sanso, pp. 326–331, Springer, Berlin.
- Andersen, O., P. Knudsen, and P. Berry (2010), The DNSC08GRA global marine gravity field from double retracked satellite altimetry, *J. Geod.*, *84*, 191–199, doi:10.1007/s00190-009-0355-9.
- Antonov, J., T. Locarnini, R. A. Boyer, A. Mishonov, and H. Garcia (2006), *World Ocean Atlas 2005*, vol. 2, *Salinity*, NOAA Atlas NESDIS, vol. 62, edited by S. Levitus, 182 pp., NOAA, Silver Spring, Md.
- Bacon, S., P. G. Myers, B. Rudels, and D. A. Sutherland (2008), Accessing the inaccessible: Buoyancy-driven coastal currents on the shelves of Greenland and eastern Canada, in *Arctic-Subarctic Ocean Fluxes: Defining the Role of the Northern Seas in Climate*, edited by R. R. Dickson, J. Meincke, and P. Rhines, chap. 28, pp. 703–722, Springer, Dordrecht, Netherlands, doi:10.1007/978-1-4020-6774-7-29.
- Bingham, R., K. Haines, and C. Hughes (2008), Calculating the ocean's mean dynamic topography from a mean sea surface and a geoid, *J. Atmos. Oceanic Technol.*, *25*, 1808–1822, doi:10.1175/2008JTECH0568.1.
- Boyer, T., S. Levitus, H. Garcia, R. Locarnini, C. Stephens, and J. Antonov (2005), Objective analyses of annual, seasonal, and monthly temperature and salinity for the world ocean on a 0.25° grid, *Int. J. Climatol.*, *25*, 931–945, doi:10.1002/joc.1173.
- Clarke, R. (1984), Transport through the Cape Farewell–Flemish Cap section, *Rapp. P. V. Reun. Cons. Int. Explor. Mer.*, *185*, 120–130.
- Colbourne, E., B. de Young, S. Narayanan, and J. Helbig (1997), Comparison of hydrography and circulation on the Newfoundland Shelf during 1990–1993 with the long-term mean, *Can. J. Fish. Aquat. Sci.*, *54*, 68–80.
- Cuny, J., P. B. Rhines, P. P. Niiler, and S. Bacon (2002), Labrador Sea boundary currents and the fate of the Irminger Sea water, *J. Phys. Oceanogr.*, *32*(2), 627–647.
- Dickson, R., B. Rudels, S. Dye, M. Karcher, J. Meincke, and I. Yashayaev (2007), Current estimates of freshwater flux through Arctic and subarctic seas, *Prog. Oceanogr.*, *73*(3–4), 210–230, doi:10.1016/j.pocean.2006.12.003.
- Fichefet, T., and M. A. M. Maqueda (1997), Sensitivity of a global sea ice model to the treatment of ice thermodynamics and dynamics, *J. Geophys. Res.*, *102*, 12,609–12,646.
- Fratantoni, P. S., and R. S. Pickart (2007), The western North Atlantic shelfbreak current system in summer, *J. Phys. Oceanogr.*, *37*(10), 2509–2533.
- Gerdes, R., W. Hurlin, and S. M. Griffies (2006), Sensitivity of a global ocean model to increased run-off from Greenland, *Ocean Modell.*, *12*(3–4), 416–435, doi:10.1016/j.oceanmod.2005.08.003.
- Heywood, K., E. McDonagh, and M. White (1994), Eddy kinetic energy of the North Atlantic subpolar gyre from satellite altimetry, *J. Geophys. Res.*, *99*, 22,525–22,539.
- Higginson, S., K. R. Thompson, and Y. Liu (2009), Estimating ocean climatologies for short periods: A simple technique for removing the effect of eddies from temperature and salinity profiles, *Geophys. Res. Lett.*, *36*, L19602, doi:10.1029/2009GL039647.

- Holliday, N. P., A. Meyer, S. Bacon, S. G. Alderson, and B. de Cuevas (2007), Retroflection of part of the east Greenland current at Cape Farewell, *Geophys. Res. Lett.*, *34*, L07609, doi:10.1029/2006GL029085.
- Huang, J., G. Fotopoulos, M. Cheng, M. Véronneau, and M. Sideris (2007), On the estimation of the regional geoid error in Canada, in *Dynamic Planet, Int. Assoc. Geod. Symp.*, vol. 130, pp. 272–279, Springer, Berlin.
- Hwang, C., H.-Y. Hsu, and R.-J. Jang (2002), Global mean sea surface and marine gravity anomaly from multi-satellite altimetry: Applications of deflection-geoid and inverse Vening Meinesz formulae, *J. Geod.*, *76*, 407–418, doi:10.1007/s00190-002-0265-6.
- Kalnay, E., et al. (1996), The NCEP/NCAR 40-year reanalysis project, *Bull. Am. Meteorol. Soc.*, *77*(3), 437–471.
- Krauss, W. (1995), Currents and mixing in the Irminger Sea and in the Iceland Basin, *J. Geophys. Res.*, *100*, 10,851–10,871, doi:10.1029/95JC00423.
- Large, W., and S. Yeager (2009), The global climatology of an interannually varying air–sea flux data set, *Clim. Dyn.*, *33*, 341–364, doi:10.1007/s00382-008-0441-3.
- Lavender, K. L., R. E. Davis, and W. B. Owens (2000), Mid-depth recirculation observed in the interior Labrador and Irminger Seas by direct velocity measurements, *Nature*, *407*(6800), 66–69, doi:10.1038/35024048.
- Lazier, J. R. N., and D. G. Wright (1993), Annual velocity variations in the Labrador Current, *J. Phys. Oceanogr.*, *23*(4), 659–678.
- Locarnini, R., A. Mishonov, J. Antonov, T. Boyer, and H. Garcia (2006), *World Ocean Atlas 2005*, vol. 1, *Temperature*, NOAA Atlas NESDIS, vol. 61, edited by S. Levitus, 182 pp., NOAA, Silver Spring, Md.
- Loder, J. W., B. Petrie, and G. Gawarkiewicz (1998), The coastal ocean off northeastern North America: A large-scale view, in *The Global Coastal Ocean: Regional Studies and Syntheses*, *Sea*, vol. 11, edited by K. H. Brink and A. R. Robinson, chap. 5, pp. 105–133, John Wiley, New York.
- Lozier, M., W. Owens, and R. Curry (1995), The climatology of the North Atlantic, *Prog. Oceanogr.*, *36*(1), 1–44.
- Lumpkin, R., and M. Pazos (2007), Measuring surface currents with Surface Velocity Program drifters: The instrument, its data, and some recent results, in *Lagrangian Analysis and Prediction of Coastal and Ocean Dynamics (LAPCOD)*, chap. 2, pp. 39–67, Cambridge Univ. Press, Cambridge, U. K.
- Madec, G., P. Delecluse, M. Imbard, and C. L evy (1998), OPA 8.1 ocean general circulation model reference manual, *Notes P ole Mod elisation 11*, 91 pp., Inst. Pierre Simon Laplace, Paris.
- Myers, P. G., C. Donnelly, and M. H. Ribergaard (2009), Structure and variability of the West Greenland Current in summer derived from 6 repeat standard sections, *Prog. Oceanogr.*, *80*(1–2), 93–112, doi:10.1016/j.pocean.2008.12.003.
- Niiler, P., and J. Paduan (1995), Wind-driven motions in the northeast Pacific as measured by Lagrangian drifters, *J. Phys. Oceanogr.*, *25*(11), 2819–2830.
- Pavlis, N., S. Holmes, S. Kenyon, and J. Factor (2008), An Earth gravitational model to degree 2160: EGM2008, paper presented at General Assembly, Eur. Geosci. Union, Vienna.
- Rio, M., and F. Hernandez (2004), A mean dynamic topography computed over the world ocean from altimetry, in situ measurements, and a geoid model, *J. Geophys. Res.*, *109*, C12032, doi:10.1029/2003JC002226.
- Sandwell, D. T., and W. H. F. Smith (2009), Global marine gravity from retracked Geosat and ERS-1 altimetry: Ridge segmentation versus spreading rate, *J. Geophys. Res.*, *114*, B01411, doi:10.1029/2008JB006008.
- Schmidt, S., and U. Send (2007), Origin and composition of seasonal Labrador Sea freshwater, *J. Phys. Oceanogr.*, *37*(6), 1445–1454, doi:10.1175/JPO3065.1.
- Smith, R. S., and J. M. Gregory (2009), A study of the sensitivity of ocean overturning circulation and climate to freshwater input in different regions of the North Atlantic, *Geophys. Res. Lett.*, *36*, L15701, doi:10.1029/2009GL038607.
- Stacey, M. W., J. Shore, D. G. Wright, and K. R. Thompson (2006), Modeling events of sea-surface variability using spectral nudging in an eddy permitting model of the northeast Pacific Ocean, *J. Geophys. Res.*, *111*, C06037, doi:10.1029/2005JC003278.
- Stouffer, R. J., et al. (2006), Investigating the causes of the response of the thermohaline circulation to past and future climate changes, *J. Clim.*, *19*(8), 1365–1387, doi:10.1175/JCLI3689.1.
- Sutherland, D. A., and R. S. Pickart (2008), The East Greenland Coastal Current: Structure, variability, and forcing, *Prog. Oceanogr.*, *78*(1), 58–77, doi:10.1016/j.pocean.2007.09.006.
- Thompson, K., D. Wright, Y. Lu, and E. Demirov (2006), A simple method for reducing seasonal bias and drift in eddy resolving ocean models, *Ocean Modell.*, *13*(2), 109–125, doi:10.1016/j.ocemod.2005.11.003.
- Thompson, K., J. Huang, M. Véronneau, D. Wright, and Y. Lu (2009), The mean surface topography of the northwest Atlantic: Comparison of estimates based on satellite, terrestrial gravity, and oceanographic observations, *J. Geophys. Res.*, *114*, C07015, doi:10.1029/2008JC004859.
- Wang, Y. (2001), GSFC 00 mean sea surface, gravity anomaly, and vertical gravity gradient from satellite altimeter data, *J. Geophys. Res.*, *106*, 31,167–31,174.
- Wright, D. G., K. R. Thompson, and Y. Lu (2006), Assimilating long-term hydrographic information into an eddy-permitting model of the North Atlantic, *J. Geophys. Res.*, *111*, C09022, doi:10.1029/2005JC003200.
- Yashayaev, I. (2007), Hydrographic changes in the Labrador Sea, 1960–2005, *Prog. Oceanogr.*, *73*(3–4), 242–276, doi:10.1016/j.pocean.2007.04.015.

S. Higginson and K. R. Thompson, Department of Oceanography, Dalhousie University, 1355 Oxford St., Halifax, NS B3H 4J1, Canada. (simon.higginson@phys.ocean.dal.ca)
 J. Huang and M. Véronneau, Geodetic Survey Division, CCRS, Natural Resources Canada, 615 Booth St., Ottawa, ON K1A 0E9, Canada.
 D. G. Wright, Fisheries and Oceans Canada, Bedford Institute of Oceanography, Dartmouth, NS B2Y 4A2, Canada.